# Implementation of Active Thermal Control (ATC) for the Soil Moisture Active and Passive (SMAP) Radiometer

Rebecca Mikhaylov[1], Eug Kwack[2], Richard French[3], Douglas Dawson[4], and Pamela Hoffman[5]
*Jet Propulsion Laboratory, California Institute of Technology, Pasadena, California, 91109*

**NASA's Earth observing Soil Moisture Active & Passive (SMAP) Mission is scheduled to launch in November 2014 into a 685 km near-polar, sun-synchronous orbit. SMAP will provide comprehensive global mapping measurements of soil moisture and freeze/thaw state in order to enhance understanding of the processes that link the water, energy, and carbon cycles. The primary objectives of SMAP are to improve worldwide weather and flood forecasting, enhance climate prediction, and refine drought and agriculture monitoring during its three year mission. The SMAP instrument architecture incorporates an L-band radar and an L-band radiometer which share a common feed horn and parabolic mesh reflector. The instrument rotates about the nadir axis at approximately 15 rpm, thereby providing a conically scanning wide swath antenna beam that is capable of achieving global coverage within three days. In order to make the necessary precise surface emission measurements from space, the electronics and hardware associated with the radiometer must meet tight short-term (instantaneous and orbital) and long-term (monthly and mission) thermal stabilities. Maintaining these tight thermal stabilities is quite challenging because the sensitive electronics are located on a fast spinning platform that can either be in full sunlight or total eclipse, thus exposing them to a highly transient environment. A passive design approach was first adopted early in the design cycle as a low-cost solution. With careful thermal design efforts to cocoon and protect all sensitive components, all stability requirements were met passively. Active thermal control (ATC) was later added after the instrument PDR to mitigate the threat of undetected gain glitches, not for thermal-stability reasons. Gain glitches are common problems with radiometers during missions, and one simple way to avoid gain glitches is to use the in-flight set point programmability that ATC affords to operate the radiometer component away from the problematic temperature zone. A simple ThermXL model (10 nodes) was developed to exercise quick trade studies among various proposed control algorithms: Modified P control vs. PI control. The ThermXL results were then compared with the detailed Thermal Desktop (TD) model for corroboration. Once done, the simple ThermXL model was used to evaluate parameter effects such as temperature digitization, heater size and gain margin, time step, and voltage variation of power supply on the ATC performance. A Modified P control algorithm was implemented into the instrument flight electronics based on the ThermXL results. The thermal short-term stability margin decreased by 10% with ATC and a wide temperature error band (±1.0ºC) compared to the original passive thermal design. However, a tighter temperature error band (±0.1ºC) increased the thermal short-term stability margin by a factor of three over the passive thermal design. The current ATC design provides robust thermal control, tighter stability, and greater in-flight flexibility even though its implementation was prompted by non-thermal performance concerns.**

[1] Instrument Thermal Engineer, Instrument Mechanical Thermal Subsystem, Mail Stop 125-123
[2] Lead Instrument Thermal Engineer, Instrument Mechanical Thermal Subsystem, Mail Stop 125-123
[3] Instrument Systems Engineer, Instrument Systems Engineering, Mail Stop 321-420
[4] Radiometer System Engineer, Instrument Systems Engineering, Mail Stop 168-314
[5] Mechanical Thermal Subsystem PDM, Instrument Mechanical Thermal Subsystem, Mail Stop 303-422

## Nomenclature

| | | |
|---|---|---|
| *ATC* | = | Active Thermal Control |
| *A2D* | = | Analog-to-Digital |
| *DTM* | = | Detailed Thermal Model |
| *GSFC* | = | Goddard Space Flight Center |
| *HITL* | = | Hardware-in-the-Loop |
| *JPL* | = | Jet Propulsion Laboratory |
| *NASA* | = | National Aeronautics and Space Administration |
| *PDM* | = | Product Delivery Manager |
| *PDR* | = | Project Design Review |
| *PI* | = | Proportional-Integral |
| *PID* | = | Proportional-Integral-Derivative |
| *P-P* | = | Peak-to-Peak |
| *RBA* | = | Reflector Boom Assembly |
| *RFE* | = | Radiometer Front End Electronics |
| *RFEA* | = | Radiometer Front End Assembly |
| *SMAP* | = | Soil Moisture Active and Passive |
| *TD* | = | Thermal Desktop |
| *TIM* | = | Technical Interface Meeting |
| *TVAC* | = | Thermal Vacuum |

## I. Introduction

The Soil Moisture Active Passive (SMAP) Mission, targeted for launch by the National Aeronautics and Space Administration (NASA) in 2014, will make global measurements of soil moisture and its freeze/thaw state by implementing an active radar and a passive radiometer that share a common L-band feed horn and a conically scanning six-meter mesh reflector antenna (Figure 1). Direct observations of soil moisture and freeze/thaw state from space will allow significantly improved estimates of water, energy, and carbon transfers between the land and the atmosphere, which in turn will lead to enhanced weather and climate forecasts, and improved flood prediction and drought monitoring capability.

Development of the SMAP instrument suite is by a NASA partnership between the Jet Propulsion Laboratory (JPL) in Pasadena, California and the Goddard Spaceflight Center (GSFC) in Greenbelt, Maryland. GSFC is responsible for the radiometer and ground science data processing system, whereas JPL is responsible for the radar, overall instrument integration, and test and pre-launch mission management. The SMAP mission formulation including the measurement approach, preliminary mission requirements, and data products were discussed, and the state-of-the-art associated with existing active/passive L-band microwave systems were summarized in previously published papers[1][2][3][4][5]. SMAP's unique nadir-spinning antenna platform generates a large swath that enables better than three day global coverage. The rotating dual-frequency radiometer and radar share a common feed, although only the radiometer has components located on the spinning platform. Signals are shared with rest of the S/C bus via slip rings.

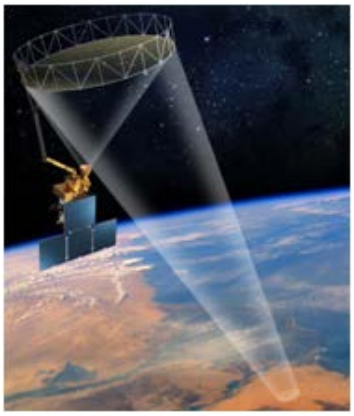

**Figure 1. SMAP observatory with spinning 6m deployable mesh reflector antenna. The active radar and passive radiometer share a common L-band feed horn.**

L-band active/passive heritage applications include the Aquarius/SAC-D mission [6][7][8][9]. The Aquarius mission, which launched in June 2011, is flying both a scatterometer (radar) built by JPL and a radiometer built by GSFC that measures sea surface salinity. While the two missions are often compared, there are some significant differences which are important to point out when discussing thermal designs: SMAP is a

spinning instrument with a single feed horn exposed to the sun; Aquarius has three feed horns that are permanently shadowed by a sun shade on a non-spinning platform; Aquarius has a 2.5m fixed antenna versus SMAP's 6m boom deployable spinning antenna; and Aquarius has a much tighter thermal stability requirement of 0.1°C over 7 days versus 0.7°C per orbit for SMAP.

The SMAP passive thermal design approach, which met all short and long-term thermal stability requirements, was published in a previous paper [10]. After Instrument PDR, Active Thermal Control (ATC) was implemented by systems engineering to mitigate the risk of radiometer gain glitches. The purpose of the ATC is to move the radiometer component away from any problematic temperature while meeting updated short and long-term stability requirements. A 10-node simple ThermXL model was developed to assist in the design. The objective of this paper is to present a description of the simple model and its use in determining the control algorithm and its effects on the SMAP radiometer temperature stability.

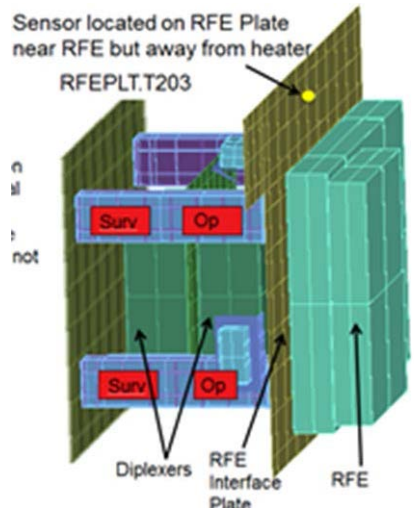


**Figure 2. Hardware configuration.**

## II. Hardware Configuration

A detailed thermal model (Thermal Desktop) was used to optimize the thermal hardware locations to control Radiometer Front End Electronics (RFE) temperature within ±2°C from the set-point. Various configurations were analyzed in the detailed model to determine the optimum location of the temperature sensor and operational heater relative to the component of interest. The temperature sensor is located near the RFE and not co-located with the heater since the RFE resides on a ribbed plate that cannot easily accommodate the heater. Heaters are installed on nearby brackets (Figure 2). When the temperature sensor was co-located with the heater on the bracket, the bracket temperature was well controlled but not the RFE. The RFE temperature was more susceptible to environmental changes over mission period due to optical property degradation and could not meet the 4°C mission-life requirement. One consideration of mounting the temperature sensor near the RFE and away from the heater is the possible overheating of components near the heater. The final

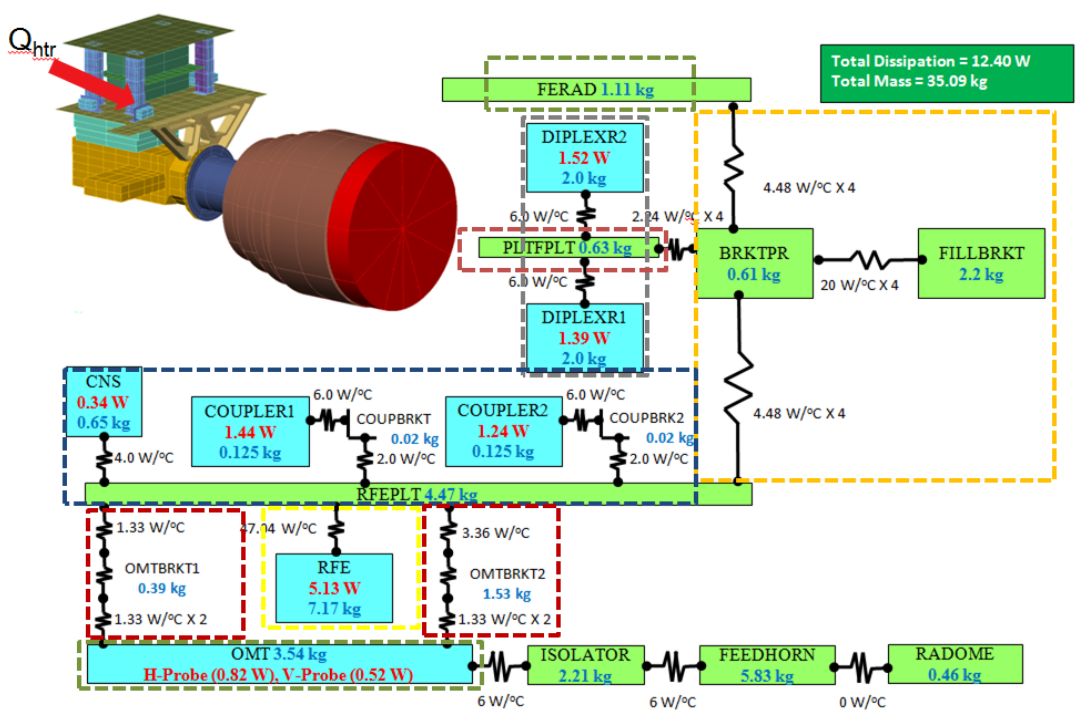


**Figure 3. Detailed Thermal Model diagram of radiometer components.**

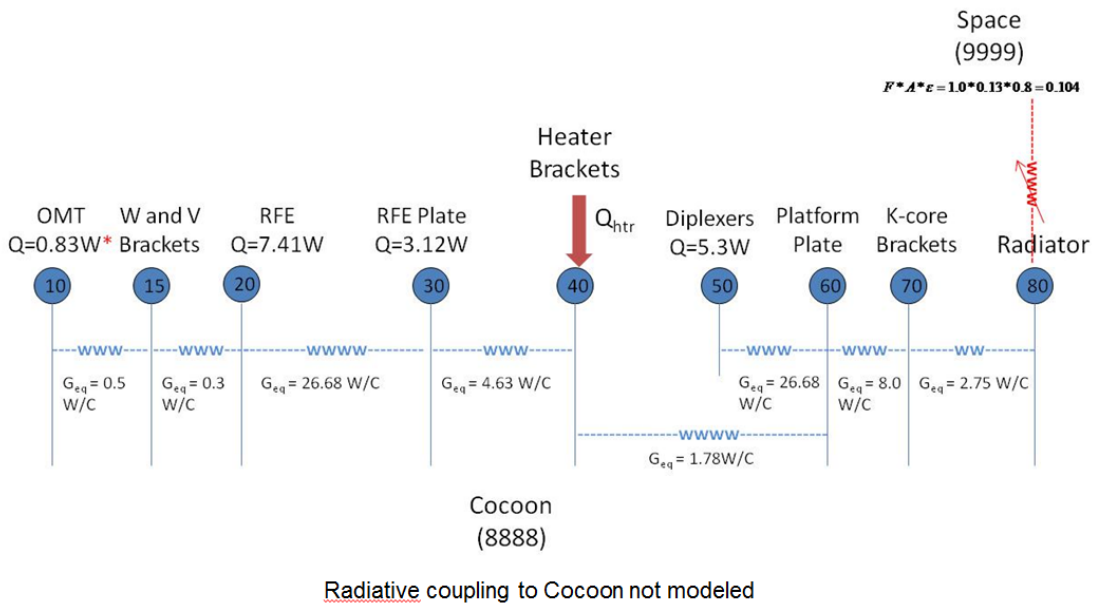


**Figure 4. Simple Thermal Model diagram of radiometer components.**

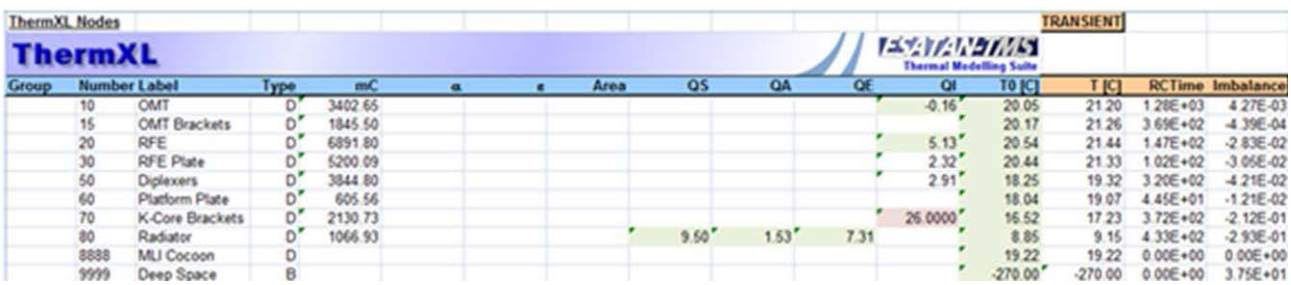

ThermXL Nodes

ThermXL

TRANSIENT

| Group | Number | Label | Type | mC | α | ε | Area | QS | QA | QE | QI | T0 [C] | T [C] | RCTime | Imbalance |
|---|---|---|---|---|---|---|---|---|---|---|---|---|---|---|---|
| | 10 | OMT | D | 3402.65 | | | | | | | -0.16 | 20.05 | 21.20 | 1.28E+03 | 4.27E-03 |
| | 15 | OMT Brackets | D | 1845.50 | | | | | | | | 20.17 | 21.26 | 3.69E+02 | -4.39E-04 |
| | 20 | RFE | D | 6891.80 | | | | | | | 5.13 | 20.54 | 21.44 | 1.47E+02 | -2.83E-02 |
| | 30 | RFE Plate | D | 5200.09 | | | | | | | 2.32 | 20.44 | 21.33 | 1.02E+02 | -3.05E-02 |
| | 50 | Diplexers | D | 3844.80 | | | | | | | 2.91 | 18.25 | 19.32 | 3.20E+02 | -4.21E-02 |
| | 60 | Platform Plate | D | 605.56 | | | | | | | | 18.04 | 19.07 | 4.45E+01 | -1.21E-02 |
| | 70 | K-Core Brackets | D | 2130.73 | | | | | | | 26.0000 | 16.52 | 17.23 | 3.72E+02 | -2.12E-01 |
| | 80 | Radiator | D | 1066.93 | | | | 9.50 | 1.53 | 7.31 | | 8.85 | 9.15 | 4.33E+02 | -2.93E-01 |
| | 8888 | MLI Cocoon | D | | | | | | | | | 19.22 | 19.22 | 0.00E+00 | 0.00E+00 |
| | 9999 | Deep Space | B | | | | | | | | | -270.00 | -270.00 | 0.00E+00 | 3.75E+01 |

**Figure 5. ThermXL implementation of simple thermal model.**

configuration was then used to determine the nodal coupling to be implemented in the simplified model (Figures 3 and 4).

## III. ThermXL Model Development

A simple 10-node ThermXL model was developed to exercise quick trade studies between the possible ATC algorithms (Figure 5). ThermXL is an Excel-based program. The worst-case thermal stability occurs at a beta angle of 58° assuming worst-case hot conditions, and a look-up table was implemented to apply varying flux values on the radiator. Worst case environmental parameters are listed in Table 1. The temperature results of the nodal and detailed models were compared by component for three different orbits (58° hot, 65° hot, and 58° cold) and verified within an acceptable error of 2°C. Additionally, the nodal and detailed models agreed within 0.18°C per orbit peak to peak (P-P) as shown in Table 2. The difference between the two models was assumed due to radiative losses from the component to the MLI cocoon, which was not represented in the simple model. The run time of the nodal model was about ten minutes versus the nearly four hours for the detailed thermal model.

## IV. ATC Algorithm Selection

Boeing developed the instrument electronic box responsible for implementing the algorithm and supplying the heater power. An initial 10 W allocation was provided with the ability to increase the ATC heater power to 26 W if necessary. In the classical closed-loop

**Table 1. SMAP environmental parameters.**

| Case | Solar Flux [W/m$^2$] | Albedo | Earth IR Flux [W/m$^2$] |
|---|---|---|---|
| Cold | 1290 | 0.25 | 190 |
| Hot | 1420 | 0.35 | 250 |

Proportional-Integral-Derivative (PID) control model [11], the heater power ($Q$) is determined by the error signal ($T_{set}$-$T$) and gain parameters ($K_p$, $K_i$, and $K_d$) as shown in Eq. (1):

$$Q \propto K_p \times (T_{set} - T) + K_i \times \int (T_{set} - T)dt + \frac{d(T_{set} - T)}{dt} \qquad (1)$$

The flight computer constantly samples the control temperature and flight software calculates the heater power. The variable, *Qmax*, cannot exceed the physical limitation determined by the spacecraft bus voltage and the heater resistance. The classical PI form has flight heritage, such as recently on the Aquarius instrument. Additionally, the simpler P-control was evaluated while introducing an offset parameter and referred to as Modified P control as shown in Eq. (2):

**Table 2. Predicted thermal stability between DTM and Nodal model with passive thermal design.**

| Component | Predicted Thermal Stability [°C/orbit P-P] | | |
|---|---|---|---|
| | Nodal Model (ThermXL) | DTM (Thermal Desktop) | Difference |
| RFE | 0.1 | 0.25 | 0.15 |
| Diplexer | 1.0 | 1.2 | 0.2 |

$$Q = K_p \times (T_{set} - T) + C_{offset} \qquad (2)$$

where $C_{offset}$ is determined by $Q_{max}/2$ and $K_p$ is $Q_{max}/(2T_{band})$ as shown in Figure 6.

Using the correlated simple model, three possible algorithms were analyzed for their stability effects on the radiometer: Proportional, Modified Proportional and Proportional-Integral (PI) as shown in Figure 7. All three algorithms were well within the 0.7°C/orbit requirement. Evaluating the benefits of each, it was determined that the Modified P control was "good enough" to meet the requirements. Since the thermal design met the requirements passively and ATC is only employed to move the component away from a temperature that has a gain glitch concern, the simpler algorithm was preferred. The algorithm is independent of time; therefore, a memory of the previous temperature is not needed. Reset of the previous temperature can often be a concern. The 10 W or 26 W heater availability did not provide enough power to fully realize the integral gain

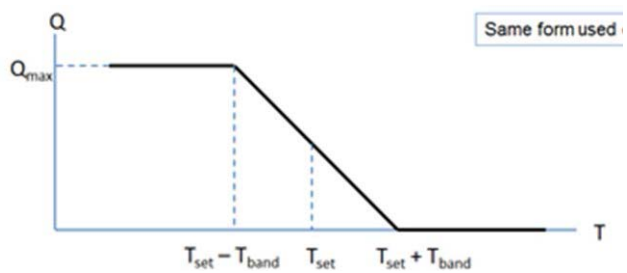


**Figure 6. Modified P-control form.**

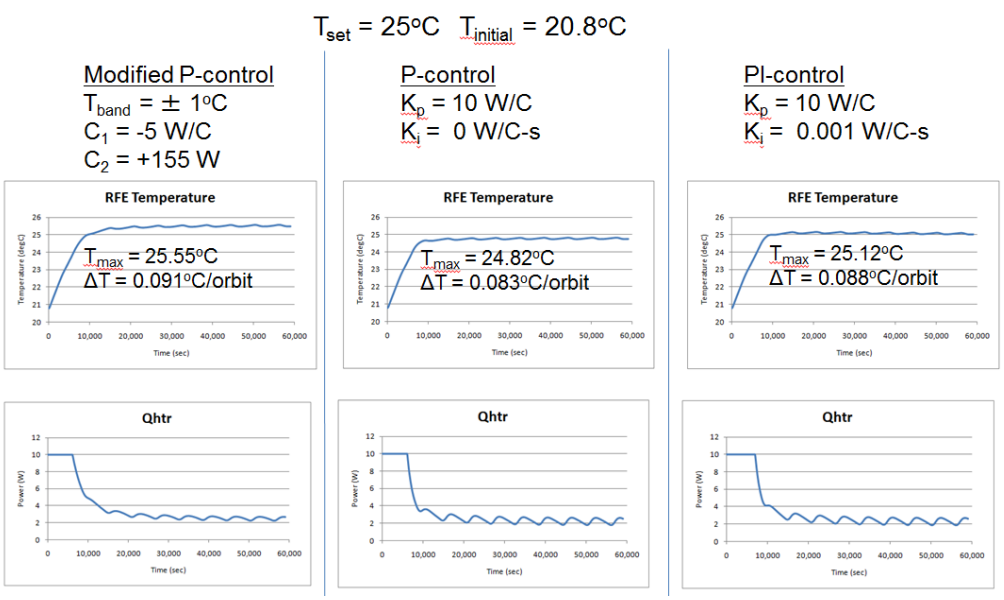


**Figure 7. ThermXL results of three different ATC algorithms.**

benefit in the PI control algorithm. The modified P control algorithm became the recommended baseline since the set temperature could be changed with only two parameters and $T_{band}$ could reduce the temperature variations during the mission. The results were presented at Technical Interface Meeting (TIM) #9 with GSFC, JPL and Boeing concurrence to proceed.

- Temperature Sensor

| Description | Comments | Value |
|---|---|---|
| Thermistor Tolerance | Tolerance included in specification to vendor. Value will be known at installation since calibration curves provided. | N/A |
| Harness | Interested in relative temperature readings as opposed to absolute. Can be calibrated out. | N/A |
| mA current source | 0.005mA value is assumed negligible. | N/A |
| 12-bit ADC | Absorbed in sampling rate. | N/A |
| 12-bit coefficients | Temperature sensor quantization error based on thermistor selected. | TS Quantization = 0.0335°C/count |
| Delays | Absorbed in sampling rate. Not concerned due to large thermal mass. | Sample Rate = 30 seconds |
| Noise | Not modeled. | N/A |

- Heater

| Description | Comments | Value |
|---|---|---|
| Heater Tolerance | Tolerance included in specification to vendor. Value will be known at installation. | N/A |
| Harness | Can be calibrated out. | N/A |

- Controller

| Description | Comments | Value |
|---|---|---|
| 12-bit DAC Voltage | Heater quantization error. Voltage variation of 29.5V ± 6%. | Heater Quantization = 0.007326V/count |

**Figure 8. List of signal-chain error sources.**

## V. ATC Implementation

Working with Boeing, a list of error sources throughout the ATC signal chain was developed (Figure 8). From the list, the team determined the credible errors that should be modeled to verify the temperature control stability. The design approach was implemented into both the detailed and nodal model and compared for the beta angle 58° hot case with ±1°C error band. The difference in the models is 0.18°C/orbit and was attributed to the modeled radiative loss to the cocoon in ThermXL. Implementing ATC does indicate an effect to the orbital stability since the thermal system was designed to meet thermal stabilities passively (Table 3). ATC with a large error band of ±1°C does increase the orbital stability by 4.5% with the detailed model and 9.4% with the simple model but it's within the 0.7°C/orbit requirement. With a tighter error band, the ATC stability can improve upon the passive design. A peer review was held to verify all system sensitivities were considered that could impact the thermal stability of the system when implementing ATC.

**Table 3. Predicted thermal stability between DTM and Nodal model with ATC and $T_{band}$ of ±1.0°C.**

| Model | Thermal Stability [°C/orbit P-P] | |
|---|---|---|
| | Passive | ATC (±1°C error band) |
| DTM | 0.337 | 0.352 |
| Nodal | 0.160 | 0.175 |

Using the simple model due to quick results (10 minutes versus 4 hours), the following effects were examined by comparing orbital stability for the worst case variation in environmental conditions (58° with hot conditions) with a temperature set point of 20°C (most likely initial set temperature):

- Quantization of temperature reading and applied voltage for heater power
- Time step
- Gain margin
- $T_{band}$ setability (error band)
- Voltage variation

### A. Quantization

The digitization step of the heater depends on the power capability and $T_{band}$. For the 26W heater, the resulting digitization effect was 0.43 W/step for 1.0°C error band (Figure 9) or 4.3 W/step for a 0.1°C error band. Almost no orbital stability effect was found – a mere increase of 0.001°C/orbit.

### B. Time Step

Due to the large mass of the system (28.0 kg), an initial time step of 30 seconds was proposed compared to the electronic box clock speed of 312 µs. Using 26 W and $T_{band}$ of 0.1°C, the temperature increased by less than 0.08°C over 30 seconds. A time step of 60 seconds was implemented to reduce model run time.

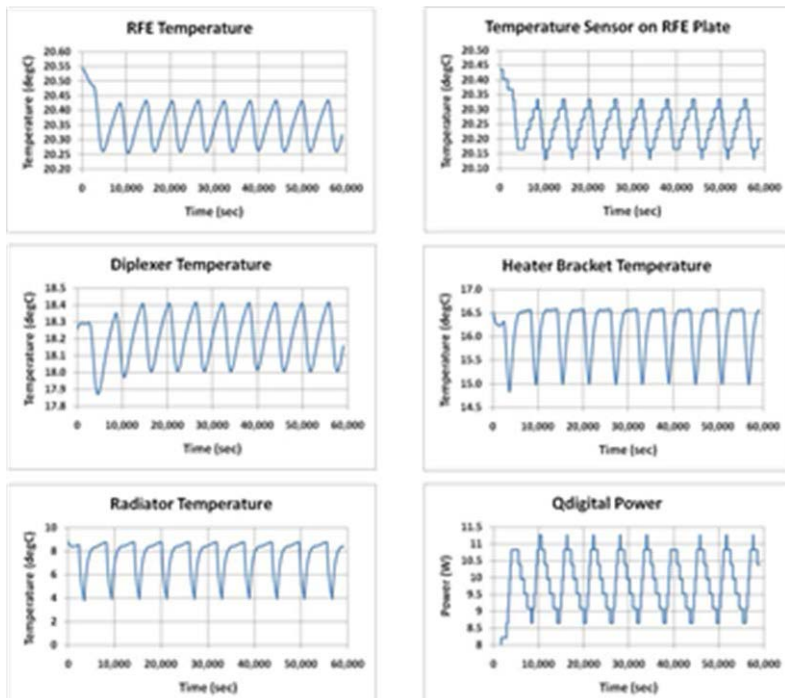


**Figure 9. Quantization effects on radiometer components and thermal stability for $T_{band}$ ±1.0°C.**

### C. Gain Margin

For the Modified P algorithm, the gain is essentially equal to the heater power. To demonstrate gain margin and its effects on temperature stability, an increase in heater power was modeled, although not physically possible. The results (Table 4) verified that the Modified P algorithm is very stable for this system, even at 4X Gain. Additionally, there is no significant improvement in thermal stability until at least 2X Gain.

**Table 4. Gain Margin.**

| $P_{Htr}$ [W] | Predicted Stability [°C/orbit P-P] | |
|---|---|---|
| | ±1°C $T_{Band}$ | ±0.1°C $T_{Band}$ |
| 0 | 0.160 | 0.160 |
| 10 | 0.166 | 0.135 |
| 26 | 0.175 | 0.0793 |
| 52 | 0.166 | 0.0349 |
| 104 | 0.137 | 0.0342 |

### D. Error Band

One benefit of the Modified P algorithm is to tighten the error band to control variations in stability using one term: $T_{band}$. A value of 1.0°C was proposed for initial use to meet the 4.0°C mission stability requirement. As expected, the orbital stability improves as $T_{band}$ is tightened. However, with a tighter $T_{band}$, temperature overshoot is larger since the temperature sensor location is away from the heater. ThermXL results confirmed the final thermal hardware configuration was acceptable but other nearby components should be monitored for possible temperature limit violations especially if the set point is near the 30°C maximum temperature limit. The diplexer is next to the heater, and its temperature overshoot is approximately 5°C since it is lightweight (Figure 10).

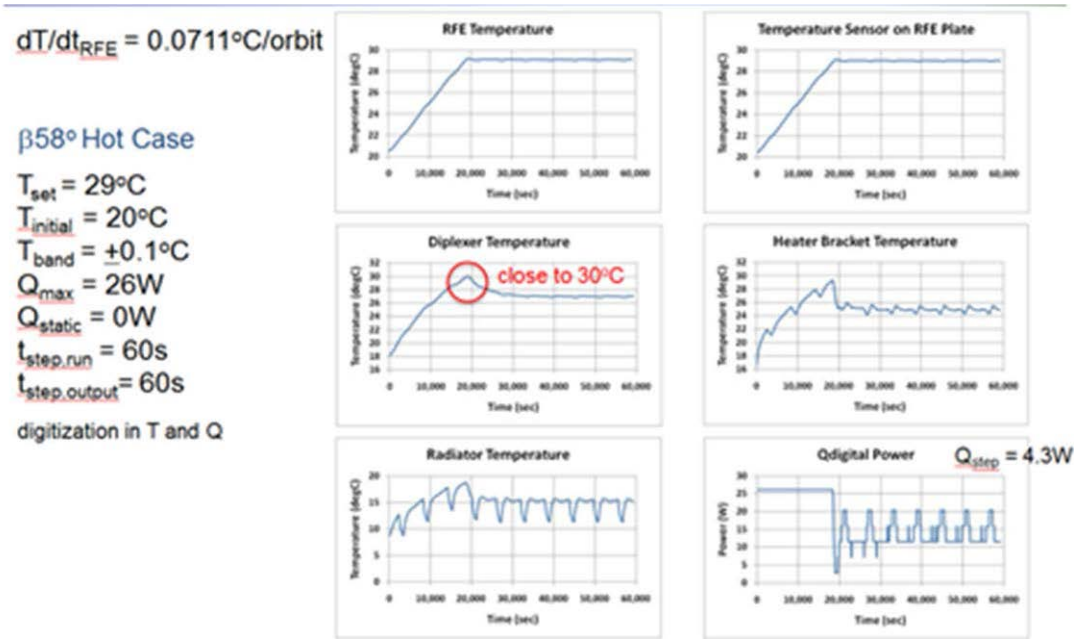


**Figure 10. Error band effect on radiometer components and thermal stability.**

### E. Voltage Variation

The electronic box specification requires 29.5 V ±6%. ThermXL was used to demonstrate a 6% fixed variation in the voltage affects the stability by approximately 0.06°C/orbit, but it can easily be absorbed since the design includes large margins (Table 5).

**Table 5. Voltage variation effects on thermal stability.**

| $Q_{max}$ | $T_{band}$ | $V_{var}$ | Overshoot Temp, °C | | | dT/dt | dT |
|---|---|---|---|---|---|---|---|
| W | ±% | ±% | Heater | Diplexer | RFE | °C/orbit | °C/orbit |
| 26 | 0.1 | 0 | 4 | 3 | 0.1 | 0.0711 | 0.04 |
| 26 | 0.1 | 6 | 6 | 4 | 0.1 | 0.111 | |
| 26 | 1.0 | 0 | 3 | 2 | 0 | 0.173 | 0.06 |
| 26 | 1.0 | 6 | 5 | 3 | 0 | 0.231 | |

### F. Testing

JPL provided two test cases to be simulated in Boeing's Hardware-in-the-Loop (HITL) architecture. The ATC portion of the HITL test objective is to verify the algorithm has been implemented as expected into the electronic box. Initial results from HITL indicated agreement between the JPL model and Boeing implementation. Additionally, the SMAP project completed Instrument thermal vacuum (TVAC) testing in November 2013 where the performance of the ATC was verified using simulation of environmental heat loads including eclipse. The ATC implementation was verified at two different set points and the transient behavior characterized during planned set temperature changes with two different error bands. The same tests will be repeated during the Observatory TVAC test scheduled for May 2014.

## VI. Conclusions

A Modified P control algorithm was implemented into the instrument flight electronics based on the results from a simple ThermXL model to operate the radiometer away from problematic temperature zones causing gain glitches. This algorithm is very stable, and over 200 ThermXL model scenarios were evaluated to demonstrate that the ATC implementation does not violate temperature stability requirements. Digitization errors in the temperature sensor reading and applied heater powers were shown to be insignificant. An advantage of the Modified P algorithm is the ability to tighten the error band to increase component stability but overshoot effects of nearby hardware should be monitored. The ATC thermal short-term stability margin (with a ±1.0°C wide temperature error band) was 10% smaller than the passive thermal design stability margin; however, tightening the temperature error band to ±0.1°C

made the ATC design greater than three times more stable than the passive thermal design. System level testing verified the ATC implementation was modeled correctly.

## Acknowledgments

The development described in this paper was carried out at the Jet Propulsion Laboratory, California Institute of Technology, under a contract with the National Aeronautics and Space Administration. The authors express their thanks to the SMAP project sponsored by NASA for supporting this effort. The authors also wish to thank several of their colleagues at JPL who were instrumental to the radiometer passive thermal control study: Matthew Stegman and Frank Ramirez for their assistance with optimizing the mechanical layout and design of the IFA, Keith English and Tenny Lim for the mechanical accommodation of the Radiometer Back End Assembly, Tim Mathews and Pete Onusconich from Boeing for the algorithm implementation into electronic box. The authors would also like to thank the following people who were involved in the SMAP ATC development and review: Eric Sunada, Ray Becker, James Borders, Nick Emis and Robert Krylo.

## References

[1] Entekhabi, D., Njoku, E.G., O'Neill, P.E., Kellogg, K., Crow, W., Edelstein, W., et. al., "The Soil Moisture Active Passive (SMAP) Mission," *Proceedings of the IEEE,* Vol. 98, No. 5, IEEE, Boston, MA, 2010, pp. 704-716.

[2] Entekhabi, D., Njoku, E., O'Neill, P., Spencer, M., Jackson, T., Entin, J., Im, E., and Kellogg, K., "The Soil Moisture Active/Passive Mission (SMAP)," *Geoscience and Remote Sensing Symposium, 2008. IGARSS 2008. IEEE International,* Vol. 3, IEEE, 2008, pp. III - 1-III - 4.

[3] Entekhabi, D., Jackson, T.J., Njoku, E., O'Neill, P., Entin, J., "Soil Moisture Active/Passive (SMAP) Mission Concept," *Atmospheric and Environmental Remote Sensing Data Processing and Utilization IV: Readiness for GEOSS II,* SPIE, Vol. 7085, 2008, pp. 70850H-1-70850H-6.

[4] Kim, S., van Zyl, J., McDonald, K., and Njoku, E., "Monitoring surface soil moisture and freeze-thaw state with the high-resolution radar of the Soil Moisture Active/Passive (SMAP) mission," *Radar Conference, 2010 IEEE,* 2010, pp. 735-739.

[5] O'Neill, P., Entekhabi, D., Njoku, E., and Kellogg, K., "The NASA Soil Moisture Active Passive (SMAP) Mission: Overview," *Geoscience and Remote Sensing Symposium (IGARSS), 2010 IEEE International,* IEEE, 2010, pp. 3236-3239.

[6] Le Vine, D.M., Lagerloef, G.S.E., Colomb, F.R., Yueh, S., and Pellerano, F., "Aquarius: An Instrument to Monitor Sea Surface Salinity From Space," *Geoscience and Remote Sensing, IEEE Transactions on,* Vol. 45, No. 7, July 2007, pp. 2040-2050.

[7] Freedman, A., McWatters, D., and Spencer, M., "The Aquarius Scatterometer: An Active System for Measuring Surface Roughness for Sea-Surface Brightness Temperature Correction," *Geoscience and Remote Sensing Symposium, 2006. IGARSS 2006. IEEE International Conference on,* IEEE, 2006, pp. 1685-1688.

[8] McWatters, D., Freedman, A., Becker, R., Granger, J., Yates, P., Franklin, B., Borders, J., Yueh, S., Spencer, M., Price, D., Fischman, M., Cheetham, C., Paller, M., Pellerano, F., and Piepmeier, J., "Architecture and Design of the Aquarius Instrument for RF and Thermal Stability," *Radar Conference, 2009 IEEE,* IEEE, 2009, pp. 1-4.

[9] Yueh, S.H., Wilson, W.J., Edelstein, W., Farra, D., Johnson, M., Pellarano, F., Le Vine, D., and Hilderbrand, P., "Aquarius Instrument Design for Sea Surface Salinity Measurements," *Geoscience and Remote Sensing Symposium, 2003. IGARSS '03. Proceedings. 2003 IEEE International,* Vol. 4, 2003, pp. 2795-2797 v.

[10]Mastropietro, A.J., Kwack, E., Mikhaylov, R., Spencer, M.W., Hoffman, P.J., Dawson, D., Piepmeier, J., Hudson, D., and Medeiros, J., "Preliminary Evaluation of Passive Thermal Control for the Soil Moisture Active Passive (SMAP) Radiometer," *41st International Conference on Environmental Systems (ICES), 2011,* AIAA 2011-5070.

[11] Ogata, K., Modern Control Engineering, 3rd ed., Prentice Hall, New Jersey, 1997, Chap. 5, pg. 218.